

A new method to measure the virial factors in the reverberation mapping of AGNs

H. T. Liu^{1,3*}, H. C. Feng^{1,2,3} and J. M. Bai^{1,3}

¹Yunnan Observatories, Chinese Academy of Sciences, Kunming, Yunnan 650011, China

²University of Chinese Academy of Sciences, Beijing 100049, China

³Key Laboratory for the Structure and Evolution of Celestial Objects, Chinese Academy of Sciences, Kunming, Yunnan 650011, China

Accepted . Received

ABSTRACT

Based on the gravitational redshift, one prediction of Einstein’s general relativity theory, of broad optical emission lines in active galactic nuclei (AGNs), a new method is proposed to estimate virial factors f in reverberation mapped masses of black holes M_{RM} . The factors f can be measured on the basis of two physical quantities, i.e. gravitational redshifts z_g and full widths at half maxima ($FWHMs$) of broad lines. The factors f are difficult to be determined due to the unclear kinematics and geometry of broad-line regions (BLRs) in AGNs. This new method is applied to narrow-line Seyfert 1 galaxy (NLS1) Mrk 110. The factor f increases with the increasing BLR size for the gravitationally redshifted broad lines He II, He I, H β and H α in Mrk 110. This trend likely results from the radiation pressure influence of accretion disc on the BLR clouds. The radiation pressure influence seems to be more important than thought usually in AGNs. Mrk 110 has $f \approx 8\text{--}16$ that are distinctly larger than the mean $\langle f \rangle \approx 1$ usually used to estimate M_{RM} in the case of $FWHM$. These larger f values will produce higher M_{RM} and lower Eddington ratios. $f = 2.9$ is derived for Seyfert 1 galaxy NGC 4593. Higher f of several tens are derived for other three mapped NLS1s. The larger factor f corresponds to the higher accretion rate for NGC 4593, Mrk 110 and other two NLS1s. The high- f values of NLS1s suggest that their BLRs are nearly face-on viewed if BLRs are disc-like.

Key words: black hole physics – galaxies: active – galaxies: nuclei – galaxies: Seyfert – quasars: emission lines.

1 INTRODUCTION

Active galactic nuclei (AGNs), such as quasars and Seyfert galaxies, can be powered by the releases of gravitational potential energy of accretion of matter onto supermassive black holes surrounded by accretion discs (Rees et al. 1982; Rees 1984). The reverberation mapping model shows that the broad emission line variations are driven by the ionizing continuum variations through the photoionization process (e.g. Blandford & McKee 1982; Peterson 1993). Broad-line region (BLR) radius r_{BLR} can be determined by time lag τ between the broad-line and continuum variations, as $r_{\text{BLR}} = \tau c$, where c is the speed of light. The reverberation mapping observations and researches have been carried out for AGNs over the last several decades (e.g. Kaspi & Netzer 1999; Kaspi et al. 2000, 2007; Peterson et al. 2005; Denney et al. 2010; Haas et al. 2011; Pozo Nuñez et al. 2012; Du et al. 2014, 2015; Pei et al. 2014; Wang et al. 2014; Barth et al.

2015; Hu et al. 2015). Recently, some reverberation mapping surveys are proposed and carried out, such as the Sloan Digital Sky Survey (SDSS) spectroscopic reverberation mapping project (Shen et al. 2015a,b, 2016) and the OzDES AGN spectroscopic reverberation mapping project (King et al. 2015). Thus, the reverberation mapping studies will be the most efficient method to estimate the black hole masses of AGNs. However, the virial factors f in the reverberation mapping mass estimation are uncertain due to the unclear kinematics and geometry of BLRs in AGNs (Peterson et al. 2004; Woo et al. 2015). The range of f appears to span several orders of magnitude (e.g. Woo & Urry 2002). An average $\langle f \rangle \approx 1$ is derived on the basis of black hole mass–stellar velocity dispersion relation ($M_{\bullet} - \sigma_{\star}$ relation) for the low redshift quiescent galaxies and/or reverberation mapped AGNs using the full widths at half maxima ($FWHMs$) of Balmer emission lines (Onken et al. 2004; Piotrovich et al. 2015; Woo et al. 2015). Constraining the virial factor f is an important task for investigating black hole mass related issues.

* E-mail: htliu@ynao.ac.cn

The BLR cloud motions of the reverberation mapped AGNs are believed and/or assumed to be dominated by the gravitational forces of the central supermassive black holes (i.e. virialized motions) (e.g. Krolik et al. 1991; Wandel et al. 1999; Krolik 2001; Barth et al. 2011; Du et al. 2014; Wang et al. 2014). Their motions generate the observed *FWHMs* of optical broad emission lines, typically thousands of km s^{-1} . The optical BLRs usually span from hundreds to thousands of gravitational radii from the central black holes for the reverberation mapped AGNs. At the huge distances, the broad lines should be redshifted due to the gravity of the central black hole. Gravitational redshift in the weak field regime establishes pure shifts of spectral features without changing their intrinsic shapes and in the strong field regime produces remarkable distortions of spectral shapes (Müller & Wold 2006). Remarkable profile distortion is a key feature of relativistic spectra of AGNs with very skewed and asymmetric line profiles, e.g. iron $\text{K}\alpha$ lines, generated in the emitting regions very close to the central black holes (e.g. Fabian et al. 1989; Popovic et al. 1995; Tanaka et al. 1995; Fabian et al. 2000; Reynolds & Nowak 2003). In literatures, there are three ways to measure the gravitational redshift z_g . First, it is measured for a broad line as a redshift difference with respect to $[\text{O III}] \lambda 5007$ (e.g. Zheng & Sulentic 1990; McIntosh et al. 1999b; Tremaine et al. 2014). Second, it is measured at different levels of the line intensity as a centroid shift with respect to the broad line peak, **eliminating all spectra with blueshifted profiles**. (Jonić et al. 2016). Third, it is measured as a broad-line **center shift of the root mean square (rms) spectrum with respect to the narrow line** (Kollatschny 2003b). **A sign of z_g was found in a statistical sense for broad $\text{H}\beta$ in the single-epoch spectra of over 20,000 quasars in the SDSS Data Release 7 (DR7) (Tremaine et al. 2014).** Jonić et al. (2016) found positive correlations, **the theoretically expected relationship such as $\Delta z \propto FWHM^2$** , between intrinsic redshifts Δz dominantly caused by the gravitational effect and widths of $\text{H}\beta$ for 209 AGNs taken from the SDSS DR7. **The redshifts of the rms profiles of broad lines and the BLR radii in Mrk 110 follow the gravitational redshift prediction (see Fig. 3 in Kollatschny 2003b).**

The reverberation mapped black hole masses are $M_{\text{RM}} \sim 10^6\text{--}10^7 M_\odot$ for Seyfert 1 galaxies (e.g. Kaspi & Netzer 1999; Kaspi et al. 2000; Peterson et al. 2005; Bentz et al. 2006; Denney et al. 2010; Haas et al. 2011; Du et al. 2014, 2015; Wang et al. 2014). Seyfert 1 galaxies have a relatively high Eddington ratio $L_{\text{bol}}/L_{\text{Edd}}$, where L_{bol} is the bolometric luminosity and L_{Edd} is the Eddington luminosity. Narrow-line Seyfert 1 galaxies (NLS1s) seem to have a more high Eddington ratio. Some NLS1s are accreting at super-Eddington accretion state. A large reverberation mapping campaign was performed by the Yunnan Observatory 2.4 m telescope from 2012 to 2013 for AGNs with super-Eddington accreting massive black holes (SEAMBHs) (Du et al. 2014; Wang et al. 2014). Hu et al. (2015) studied the properties of emission lines for 10 NLS1s with SEAMBHs, and found the redshifts and/or blueshifts of $\text{H}\beta$ and Fe II . The inflow and outflow of BLR gas may generate redshifts and blueshifts, respectively. Kollatschny (2003a) ruled out that radial inflow or outflow motions are

dominant in the BLR of Seyfert 1 galaxy Mrk 110. The $\text{H}\beta$ line in Seyfert 1 galaxy Mrk 50 has an origin in a BLR dominated by orbital motion rather than infall or outflow (Barth et al. 2011). Kollatschny (2003b) found the gravitationally redshifted broad emission lines He II , He I , $\text{H}\beta$ and $\text{H}\alpha$. The BLRs will "breathe" with the central radiation variations (e.g. Barth et al. 2015, references therein). The breaths occur on short timescales of days to weeks in response to continuum variations, and the broad-line shifts of $\sim 100 \text{ km s}^{-1}$ were found over about one month. The breathing effects of BLRs on the broad-line shifts might be eliminated in the rms and mean spectra of the reverberation mapped AGNs. The gravitational redshifts of the broad lines in Mrk 110 were determined based on the rms spectra (Kollatschny 2003b). The redshifted $\text{H}\alpha$ and $\text{H}\beta$ broad lines were found with the rms spectra for Seyfert 1 galaxy NGC 4593, and their redward shifts might be interpreted as the gravitational redshift (Kollatschny & Dietrich 1997). In this paper, we derive a new method to estimate the virial factors f with gravitationally redshifted broad optical emission lines in AGNs, and apply this new method to several reverberation mapped Seyfert 1 galaxies.

The structure of this paper is as follows. Section 2 presents the method. Section 3 describes the application to Mrk 110. Section 4 is for the application to NGC 4593. Section 5 is for the applications to Mrk 493, *IRAS* 04416 and Mrk 42. Section 6 presents discussion and conclusions. Throughout this paper, we use the standard cosmology with $H_0 = 70 \text{ km s}^{-1} \text{ Mpc}^{-1}$, $\Omega_{\text{M}} = 0.3$, and $\Omega_{\Lambda} = 0.7$ (Spergel et al. 2003; Riess et al. 2004).

2 METHOD

The BLRs are distant from the central black holes for the reverberation mapped AGNs. The Schwarzschild metric will be reasonable to describe the space-time around the BLRs. The Kerr metric and the Schwarzschild metric have the identical effect on the gravitational redshift at distances larger than about one hundred gravitational radii from the black holes (see Fig. 9 in Müller & Wold 2006). The Schwarzschild space-time is

$$\begin{aligned} ds^2 &= -g_{\mu\nu} dx^\mu dx^\nu \\ &= \left(1 - \frac{2GM_\bullet}{c^2 r}\right) c^2 dt^2 - \left(1 - \frac{2GM_\bullet}{c^2 r}\right)^{-1} dr^2 \\ &\quad - r^2 d\theta^2 - r^2 \sin^2 \theta d\varphi^2, \end{aligned} \quad (1)$$

where G is the gravitational constant, c is the speed of light, and M_\bullet is the mass of black hole. The ratio of the frequency of atomic transition ν_e at the BLR radius r_{BLR} to the frequency ν_o observed at infinite distance is (static cloud)

$$\begin{aligned} \frac{\nu_o}{\nu_e} &= \frac{(-g_{00})_{r_{\text{BLR}}}^{1/2}}{(-g_{00})_\infty^{1/2} c} \\ &= \left(1 - \frac{2GM_\bullet}{c^2 r_{\text{BLR}}}\right)^{1/2}, \end{aligned} \quad (2)$$

where $(-g_{00})_\infty = 1$ at the observer's frame. So, the gravitational redshift is

$$z_g = \frac{\nu_e}{\nu_o} - 1 = \left(1 - \frac{2GM_\bullet}{c^2 r_{\text{BLR}}}\right)^{-1/2} - 1. \quad (3)$$

The black hole mass M_\bullet is

$$M_\bullet = \frac{1}{2} G^{-1} c^2 r_{\text{BLR}} [1 - (1 + z_g)^{-2}], \quad (4)$$

and the first order approximation is

$$M_\bullet \cong G^{-1} c^2 z_g r_{\text{BLR}}, \quad (5)$$

if $z_g \ll 1$. Equation (5) was used to estimate M_\bullet in Kollatschny (2003b) and Zheng & Sulentic (1990).

In general, the gravitational redshift z_g is derived from the redshift differences of the broad emission lines relative to the narrow emission lines. As the narrow lines do not appear in the spectrum containing the broad lines, the redshift differences $\Delta z_{i,j} = z_i - z_j = z_{g,i} - z_{g,j}$ for the broad lines i and j are used to estimate M_\bullet . And then we have

$$\begin{aligned} \Delta z_{i,j} &= \left(1 - \frac{2GM_\bullet}{c^2 r_{\text{BLR},i}}\right)^{-1/2} - \left(1 - \frac{2GM_\bullet}{c^2 r_{\text{BLR},j}}\right)^{-1/2} \\ &\cong \frac{GM_\bullet}{c^2} \left(\frac{1}{r_{\text{BLR},i}} - \frac{1}{r_{\text{BLR},j}}\right), \end{aligned} \quad (6)$$

where $r_{\text{BLR}} \gg r_g = GM_\bullet/c^2$ (r_g is the gravitational radius), and

$$M_\bullet \cong G^{-1} c^2 \Delta z_{i,j} \left(\frac{1}{r_{\text{BLR},i}} - \frac{1}{r_{\text{BLR},j}}\right)^{-1}, \quad (7)$$

where $r_{\text{BLR},i}$ and $r_{\text{BLR},j}$ correspond to the broad lines i and j , respectively. Black hole mass can be determined based on the virial theorem for the reverberation mapped AGNs:

$$M_{\text{RM}} = f \frac{v_{\text{FWHM}}^2 r_{\text{BLR}}}{G}, \quad (8)$$

where v_{FWHM} is the *FWHM* of broad emission line (Peterson et al. 2004). If both of the mapping method and the gravitational redshift method measure the mass M_\bullet , the mapping mass M_{RM} is equal to the gravitational redshift mass M_{grav} derived from equation (4) for each AGN. Thus, we have the virial factor

$$f = \frac{1}{2} \frac{c^2}{v_{\text{FWHM}}^2} [1 - (1 + z_g)^{-2}], \quad (9)$$

for the reverberation mapped AGNs. This gravitational redshift approach will be a terse method to estimate the virial factor f in equation (8). If the BLRs have disc-like geometry with an inclination θ , $f = 1/4 \sin^2 \theta$ (McLure & Dunlop 2001). As $f = 1$, $\theta = 30$ degrees.

3 APPLICATION TO MRK 110

The shifts of the rms line centers (uppermost 20%) with respect to the narrow lines are identified as the gravitational redshifts (Kollatschny 2003b). The mean profiles of the broad lines are not shifted with respect to the forbidden narrow lines on the other hand. Therefore, the differential shifts of the rms

profiles with respect to the narrow lines are identical to their shifts with respect to the mean profiles (Kollatschny 2003b). The virial factor f is derived by equation (9) for broad lines He II, He I, H β and H α (see Table 1). Considering the errors of v_{FWHM} and z_g , the f distribution is generated with equation (9) by 10^4 realizations of Monte Carlo simulation. The mean and standard deviation of this distribution are regarded as the expectation and uncertainty of f , respectively. The helium and hydrogen lines have $f \approx 8$ –16 that are larger than the average $\langle f \rangle \approx 1$ usually accepted for the reverberation mapped AGNs. The f values of the helium lines are slightly smaller than those of the hydrogen lines. If the BLRs are disc-like, their inclination angles θ are ≈ 7 –10 degrees (see Table 1). These inclination angles indicate the nearly face-on view of the disc-like BLRs, and also confirm the nearly face-on view of accretion disc in Mrk 110 suggested by Kollatschny (2003a,b). The four broad lines He II, He I, H β and H α have obvious stratification in the BLRs, as predicted by the virial theorem (Kollatschny 2003b), and are from the near to the distant away from the central black hole. These stratification BLRs are dominated by the gravity of the central supermassive black hole. Mrk 110 will have the virial velocity $v_c^2 = GM_\bullet r_{\text{BLR}}^{-1}$ and $v_{\text{FWHM}}^2 \propto v_c^2 \propto r_{\text{BLR}}^{-1}$. We have $f \cong z_g c^2 / v_{\text{FWHM}}^2$ because $z_g \ll 1$ in equation (9) for Mrk 110, and then $f \propto z_g r_{\text{BLR}} \propto M_\bullet$ (see equation [5]). M_\bullet can be regarded as a constant in observation periods for individual AGNs. So, f is independent of r_{BLR} . However, there is a positive correlation between $\log f$ and $\log r_{\text{BLR}}$ for Mrk 110 (see Figure 1). This increasing trend of $\log f$ versus $\log r_{\text{BLR}}$ is inconsistent with the independent prediction of the virial theorem.

There are two paths to estimate black hole mass, i.e. the single broad-line estimation (equation [4]) and the broad-line-to-broad-line comparison (equation [7]). The mass M_{grav} is estimated for the broad lines He II, He I, H β and H α (see Tables 1 and 2). According to basic error propagation used conventionally in the reverberation mapping, we estimate the uncertainty of M_{grav} from the errors of r_{BLR} and z_g . Each M_{grav} value in Table 2 will correspond two M_{grav} values in Table 1 because equation (7) is based on two broad lines. Comparison between these two kinds of masses shows that the masses estimated by the two paths are consistent with each other (see Figure 2). This agreement indicates that the broad-line-to-broad-line comparison path is feasible and reliable to estimate M_{grav} . These black hole masses in Tables 1 and 2 are also consistent with the mean mass of $\log M_{\text{grav}}/M_\odot = 8.15$ derived in Kollatschny (2003b). The broad-line-to-broad-line comparison path is without the difficulty of the reference of the gravity redshift of broad line as in the single broad-line path, such as the blueshift of the narrow line [O III] $\lambda 5007$. This narrow line blueshift will generate equivalently a broad-line redshift as the blueshifted narrow line is used as the reference to estimate z_g . In principle, the broad-line-to-broad-line comparison path could eliminate mostly the line shift influence due to the BLR "breath". In the terms of the two factors, this broad-line-to-broad-line comparison path seems to be better than the single broad-line path to estimate M_{grav} as there are several broad lines in spectra. So, equation (7) is appropriate to estimate M_{grav} for broad-line AGNs. Equation (4) is appropriate for a single broad line except for the

Table 1. Virial factors, gravitational masses, and accretion disc inclinations of Mrk 110 and NGC 4593

Object	Line	$\frac{FWHM}{\text{km s}^{-1}}$	z_g	τ (days)	$\log \frac{M_{\text{grav}}}{M_{\odot}}$	f	θ°
(1)	(2)	(3)	(4)	(5)	(6)	(7)	(8)
Mrk 110	He II $\lambda 4686$	4444 ± 200	0.00180 ± 0.00020	3.9 ± 2	8.09 ± 0.23	8.23 ± 1.18	10.12 ± 0.74
Mrk 110	He I $\lambda 5876$	2404 ± 100	0.00062 ± 0.00020	10.7 ± 6	8.07 ± 0.28	9.70 ± 3.21	9.24 ± 1.56
Mrk 110	H β $\lambda 4861$	1515 ± 100	0.00039 ± 0.00017	24.2 ± 4	8.22 ± 0.20	15.65 ± 6.79	7.26 ± 1.68
Mrk 110	H α $\lambda 6563$	1315 ± 100	0.00025 ± 0.00017	32.3 ± 5	8.15 ± 0.30	14.59 ± 8.27	7.52 ± 2.79
NGC 4593	H α $\lambda 6563$	3400 ± 200	0.00037 ± 0.00010	3.8 ± 2.0	7.39 ± 0.26	2.91 ± 0.86	17.04 ± 2.60

Notes: Column 1: object names; Column 2: emission line names; Column 3: $FWHM$ s of broad emission lines in the rms spectra; Column 4: gravitational redshifts; Column 5: time lags of lines in the rest frame; Column 6: gravitational masses derived from equation (4); Column 7: the virial factors; Column 8: inclinations if BLRs have disc-like geometry.

Table 2. M_{grav} from broad lines for Mrk 110

Line	He I $\lambda 5876$	H β $\lambda 4861$	H α $\lambda 6563$
(1)	(2)	(3)	(4)
He II $\lambda 4686$	8.10 ± 0.39	8.06 ± 0.28	8.08 ± 0.26
He I $\lambda 5876$		7.89 ± 0.66	8.02 ± 0.48
H β $\lambda 4861$			8.38 ± 0.82

Notes: gravitational masses derived from equation (7) and scaled as $\log \frac{M_{\text{grav}}}{M_{\odot}}$.

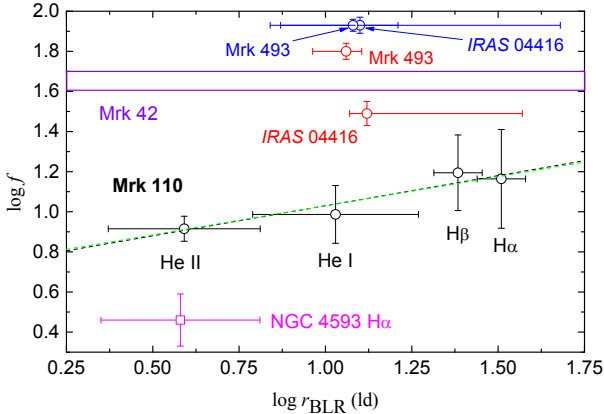


Figure 1. $\log f$ vs $\log r_{\text{BLR}}$. Black circles are for Mrk 110. Circles in color are for SEAMBH AGNs. Red circles denote the H β line, and blue circles denote the Fe II line. Violet lines denote the f values for Mrk 42. Black line is the best fit to the black circles with a Pearson's correlation coefficient $r = 0.948$ at the confidence level of 94.8 percent [$y = 0.73(\pm 0.08) + 0.30(\pm 0.07) \times x$]. Green line is the best fit to the black circles and uncertainties in x and y by the "FITEXY" estimator (Press et al. 1992) with a chi-square $\chi^2 = 0.180$ and a goodness-of-fit $Q = 0.914$ [$y = 0.74(\pm 0.21) + 0.29(\pm 0.22) \times x$].

blueshift issue of the narrow line used as the reference to estimate z_g .

4 APPLICATION TO NGC 4593

NGC 4593 is a nearby Seyfert 1 galaxy. This object is a sub-Eddington accretor with an average $\dot{M} = 0.08$, where dimensionless accretion rate $\dot{M} = \dot{M}_\bullet / L_{\text{Edd}} c^{-2}$ and \dot{M}_\bullet is the mass accretion rate (Du et al. 2015). Early reverberation mapping yielded a lag of four days indicating a very compact BLR (Dietrich et al. 1994). Recent reverberation mappings confirm this lag of four days (e.g. Du et al. 2015,

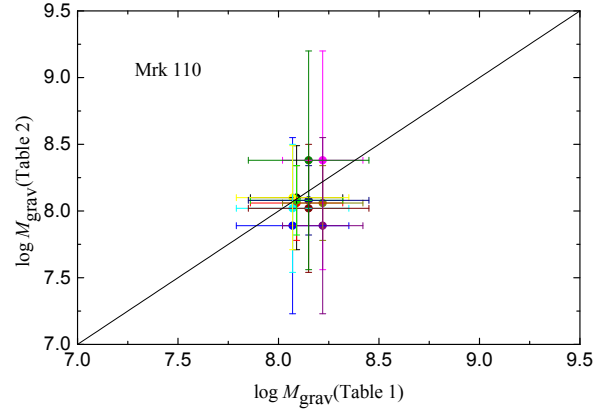


Figure 2. Comparison between M_{grav} derived from equations (4) and (7). Black line is $y = x$.

references therein). Kollatschny & Dietrich (1997) found the redshifted H α and H β broad lines with the rms spectra, and thought that the observed redshift might be interpreted as the gravitational redshift. The central component of H α is redshifted by $110 \pm 30 \text{ km s}^{-1}$ and the H β rms spectrum shows a redshift of the same order. We have $FWHM = 3400 \pm 200 \text{ km s}^{-1}$ for both of the H α rms and mean spectra. The relevant physical quantities of H α are listed in Table 1. A mass $M_{\text{grav}} = 2.5(\pm 1.5) \times 10^7 M_{\odot}$ is derived from equation (4). A value $f = 2.9$ is obtained for the redshifted H α line. This f value is slightly higher than the average $\langle f \rangle \approx 1$ usually accepted. The value $f = 2.9$ is smaller than those of Mrk 110. In plot of $\log f$ versus $\log r_{\text{BLR}}$, NGC 4593 is below the straight line best fit to Mrk 110 (see Figure 1). Mrk 110 has an average $\dot{M} = 5.89$ (Du et al. 2015). The difference of position in plot of $\log f$ versus $\log r_{\text{BLR}}$ may be from the difference of \dot{M} . If the BLR is disc-like in NGC 4593, the BLR inclination angle is ≈ 17 degrees. The inclination effect will generate different f even for the same disc-like BLR (e.g. McLure & Dunlop 2001). Another possible explanation of the different f is that the accretion rate \dot{M} dominates the factor f because both of $f = 2.9$ and $\dot{M} = 0.08$ in NGC 4593 are smaller compared to both of $f = 14.6$ and $\dot{M} = 5.89$ in Mrk 110 for H α . We have a normalization of \dot{M} relative to f $\dot{M}_f = 0.03$ and 0.40 for NGC 4593 and Mrk 110, respectively. This normalized value \dot{M}_f reflects the composite effects of the central black hole gravity, the central radiation pressure and the kinematics and geometry of BLR. Mrk 110 has higher \dot{M}_f and f than does NGC 4593.

5 APPLICATIONS TO MRK 493, IRAS 04416 AND MRK 42

Hu et al. (2015) studied the properties of emission lines for 10 NLS1s. Mrk 493, IRAS 04416+1215 and Mrk 42 have the redward shifted optical Fe II and H β lines with respect to [O III] λ 5007. The virialized motions of BLR clouds are also assumed to estimate M_{RM} in the reverberation mapping of H β for these NLS1s (Du et al. 2014; Wang et al. 2014). So, the redward shifts of H β and Fe II may be the gravitational redshift. The Fe II lag is consistent with the H β lag for the same source (see Table 3). Mrk 493 and Mrk 42 have the Fe II *FWHMs* indistinguishable from the H β *FWHMs*. The Fe II *FWHM* is slightly smaller than the H β *FWHM* in IRAS 04416+1215. It seems that there are no obvious stratification in BLRs for Mrk 493, IRAS 04416 and Mrk 42. Here, we regard these redward shifts of the Fe II and H β lines as the gravitational redshift. The details for these three NLS1s are listed in Table 3. The factors f and masses M_{grav} are estimated by equations (9) and (4), respectively. These three NLS1s have f higher than Mrk 110 (see Figure 1). The f values of these NLS1s are much larger than the average $\langle f \rangle \approx 1$ accepted usually in the reverberation mapping. The more high- f values imply that NLS1s may have higher black hole masses than M_{RM} in the case of $\langle f \rangle \approx 1$, and the higher masses will decrease the Eddington ratios. This is very similar to the case of Mrk 110 with a mean $f \approx 12$, which will make M_{RM} increase by an order of magnitude with respect to the mass estimated with $\langle f \rangle \approx 1$.

These NLS1s and Mrk 110 have comparable r_{BLR} and M_{grav} , but distinctly different f (see Figure 1). These behaviors might be from the difference between accretion states. Mrk 493 and IRAS 04416 have $\dot{M} = 75.9$ and $\dot{M} = 426.6$, respectively (Du et al. 2015). Mrk 493 and IRAS 04416 have a mean $f = 73.3$ and $f = 58.7$, respectively. Thus, Mrk 493 and IRAS 04416 have $\dot{M}_f = 1.04$ and $\dot{M}_f = 7.27$, respectively. Mrk 110 has a mean $f = 12.0$ and $\dot{M}_f = 0.49$. In terms of \dot{M} and \dot{M}_f , Mrk 493 and IRAS 04416 are at higher accretion states than Mrk 110. The higher accretion rate seems to correspond to the larger f . The higher accretion rate will produce the higher radiation pressure on the BLR clouds. The higher radiation pressure will counteract a more proportion of gravity of black hole, and then the BLR clouds will have a smaller virial velocity, i.e. v_{FWHM} will decrease if the radiation pressure increases, given that the BLR clouds are in virialized motions. Ultimately, the radiation pressure will influence M_{RM} . Thus, the factor f estimated by equation (9) will be higher than that expected from the virial assumption without considering the radiation pressure. If NLS1s have a disc-like BLR, there are inclinations of 3–5 degrees, indicating a nearly face-on view, for these three NLS1s.

A higher mass $\log M_{\text{grav}}/M_{\odot} \approx 9.5$ is estimated by equation (7) for IRAS 04416. A very large error of $\log M_{\text{grav}}/M_{\odot}$ will be generated by the larger error of τ ($r_{\text{BLR}} = c\tau$) (see Table 3). This larger mass is on the same order of magnitude as the mass estimated by equation (4) for Fe II when considering its errors. This means that the single broad-line path and the broad-line-to-broad-line comparison path are equally applicable to estimating M_{grav} for IRAS 04416. A further test is needed in the future with high quality time lags of H β and Fe II to check the validity of these two paths. The current result indicates that the red-

ward shifts of H β and Fe II with respect to [O III] are reliable to be used as the gravitational redshift, i.e. the [O III] line redshift can be regarded as the systemic redshift. Equation (7) cannot be applied to Mrk 493. The applications to Mrk 110, IRAS 04416 and Mrk 493 show that the broad-line-to-broad-line comparison path is more applicable to those AGNs with obvious stratification in BLRs, such as Mrk 110.

6 DISCUSSION AND CONCLUSIONS

Müller & Wold (2006) used the Kerr ray tracing simulations to study the gravitational redshifts of Mrk 110. When $r_{\text{BLR}} \gtrsim 100 r_g$, the simulation results for stationary rotating emitters are nearly identical to, within the errors, those for static emitters in the Kerr space-time and the Schwarzschild space-time (see Fig. 9 in Müller & Wold 2006). Mrk 110 has $r_{\text{BLR}} \sim 560\text{--}4000 r_g$ for the broad lines He II, He I, H β and H α . So, it is reasonable and reliable to estimate f and M_{grav} by using the formulas in section 2. The gravitational redshift effect will exist in the broad lines as long as the BLRs in AGNs surround the central supermassive black holes. However, the gravitational redshift is not always observable due to several factors. The first factor is the observational accuracies, such as the low signal to noise ratios. The second is the breathing of BLRs that shifts the broad lines redward or blueward. The rms and mean spectra may eliminate this breathing effect of BLRs on z_g . **The redshifts and BLR radii of broad lines follow the gravitational redshift prediction in Mrk 110 (see Fig. 3 in Kollatschny 2003b), and this following shows that the broad line shifts are dominated by the gravitational redshift for the rms spectra.** The rms spectra were used to measure z_g of the broad lines in Mrk 110 (Kollatschny 2003b) and NGC 4593 (Kollatschny & Dietrich 1997). The third is that the inflow may also produce the broad line redshifts relative to the narrow lines. The reverberation mapping assumes that the BLR cloud motions meet the virial theorem. It was ruled out that radial inflow or outflow motions are dominant in the BLRs of NGC 4593 (Kollatschny & Dietrich 1997), Mrk 110 (Kollatschny 2003a), Mrk 50 (Barth et al. 2011) and Mrk 1044 (Du et al. 2016). The fourth is the other broad and/or narrow lines blended with the target broad line, which may make z_g unobservable. These blended line components will influence the *FWHM* and centroid of broad line in the rms spectra (e.g. Barth et al. 2015). So, these blended line components may make it difficult to measure z_g .

Jonić et al. (2016) eliminated all spectra with blueshifted line profiles. In these spectra, some other effects (e.g. outflows) could be more dominant than the gravitational effects, so they are not convenient for this research of the gravitational redshifts in the lines. It is difficult to state that all spectra with strong outflow influence are completely eliminated, since it is possible that the combination of the outflow and gravitational redshift produce symmetrical line shape (Jonić et al. 2016). They have obtained H β spectrum in 209 AGNs taken from the SDSS DR7, and their sample number is about 1% of that in Tremaine et al. (2014), in which there are over 20,000 quasars with broad H β in the single-epoch

Table 3. Virial factors, masses, and accretion disc inclinations of NLS1s derived from H β and Fe II lines

Object	Line	$\frac{FWHM}{\text{km s}^{-1}}$	z_g	τ (days)	$\log \frac{M_{\text{grav}}}{M_{\odot}}$	f	θ°
(1)	(2)	(3)	(4)	(5)	(6)	(7)	(8)
<i>IRAS</i> 04416+1215	H β	1522 \pm 44	0.00080 \pm 0.00010	13.3 $^{+13.9}_{-1.4}$	8.27 $^{+0.46}_{-0.07}$	31.14 \pm 4.29	5.14 \pm 0.37
Mrk 42	H β	802 \pm 18	0.00029 \pm 0.00006			40.60 \pm 8.60	4.50 \pm 0.55
Mrk 493	H β	778 \pm 12	0.00042 \pm 0.00004	11.6 $^{+1.2}_{-2.6}$	7.93 $^{+0.06}_{-0.11}$	62.44 \pm 6.26	3.63 \pm 0.19
Mrk 486	H β	1942 \pm 67	-0.00015 \pm 0.00003	23.7 $^{+7.5}_{-2.7}$			
<i>IRAS</i> 04416+1215	Fe II	1313 \pm 50	0.00165 \pm 0.00007	12.6 $^{+16.7}_{-6.7}$	8.56 $^{+0.58}_{-0.23}$	86.31 \pm 7.56	3.09 \pm 0.14
Mrk 42	Fe II	787 \pm 16	0.00035 \pm 0.00006			50.94 \pm 8.97	4.02 \pm 0.38
Mrk 493	Fe II	780 \pm 9	0.00057 \pm 0.00003	11.9 $^{+3.6}_{-6.5}$	8.08 $^{+0.13}_{-0.24}$	84.25 \pm 4.85	3.12 \pm 0.09
Mrk 486	Fe II	1790 \pm 88	0.00032 \pm 0.00011	17.3 $^{+5.8}_{-3.7}$	7.99 $^{+0.21}_{-0.18}$	8.98 \pm 3.21	9.60 \pm 1.73

Notes: Same as in Table 1 except for Column 3: the H β $FWHM$ s are from the mean spectra, and the Fe II $FWHM$ s are the means and standard deviations obtained from the measurements of individual-night spectra (Hu et al. 2015).

spectrum taken from the SDSS DR7. So, it is difficult to measure z_g due to some other effects, e.g. outflows, and the chance of finding the gravitational redshift is very low. Since the combination of the outflow and gravitational redshift is possible, the application objects may be influenced by this combination. The broad-line-to-broad-line comparison path, equation (7), may eliminate mostly the underlying effects (inflows or outflows) by using different broad lines rather than single broad line. Comparisons of masses derived from equations (7) and (4) for Mrk 110 show that the two kinds of black hole masses are consistent with each other within uncertainties (see Figure 2). This indicates that the underlying effects are weaker than the gravitational redshift effect, and should be mostly eliminated by the broad-line-to-broad-line comparison path. For *IRAS* 04416, mass derived from equation (7) is larger than those from equation (4), but on the same order of magnitude, considering uncertainties. This implies for *IRAS* 04416 that the underlying effects are notable, but weaker than the gravitational redshift effect, and also it should be mostly eliminated by equation (7). Though, equations (4), (5) and (9) are not applicable to the blueshifted lines (because the blueshift effect is not eliminated in the case of the single broad line), equation (7) may be applicable. NLS1 Mrk 486 has the redshifted Fe II broad line (redshifted on $\pm 1\sigma$) and the blueshifted H β broad line (blueshifted on $\pm 1\sigma$) (see Table 2 in Hu et al. 2015). Mrk 486 has $\log M_{\text{grav}}/M_{\odot} = 8.72^{+0.66}_{-0.38}$ derived from equation (7) and $\log M_{\text{grav}}/M_{\odot} = 7.99^{+0.21}_{-0.18}$ from equation (4). These two masses are on the same order of magnitude. In terms of the combination of the outflow and the gravitational redshift effect, the outflow effect may be not strong, but more notable relative to the gravitational redshift effect in Mrk 486. The virial factor $f \approx 9$ is estimated by equation (9) and Fe II. This value might be the lower limit of f , for that the redshifted Fe II may be not purely due to the gravitational redshift effect.

In the absence of the radiation pressure on the BLR clouds of AGNs with masses M_{\bullet} , there is $v_c^2 = GM_{\bullet}/r_{\text{BLR}} = r_{\text{BLR}}^{-1}(r_g)c^2$, where $r_{\text{BLR}}(r_g)$ is in units of r_g . At the same time, $v_{\text{FWHM}}^2 \propto v_c^2 \propto r_{\text{BLR}}^{-1}(r_g)$. Equations (4) and (9) are combined to give $f = GM_{\bullet}/(r_{\text{BLR}}v_{\text{FWHM}}^2) \propto r_{\text{BLR}}^{-1}(r_g)/v_{\text{FWHM}}^2 \propto C$, where C is independent of r_{BLR}

and M_{\bullet} . However, Figure 1 shows the evidence of the increasing trend of f with r_{BLR} . So, this problem may result from the ignoring of the radiation pressure of accretion disc on these clouds. The radiation pressure will push these clouds towards the larger radius compared to the BLR radius in the absence of the radiation pressure. Thus, $v_c^2 \neq GM_{\bullet}/r_{\text{BLR}}$ in the presence of the radiation pressure. We will have $v_{\text{cr}}^2 = GM_{\bullet}/r_{\text{BLR}}/(r_{\text{BLR}}/ld)^{\alpha}$ instead of $v_c^2 = GM_{\bullet}/r_{\text{BLR}}$ for AGNs with luminous accretion discs, where $(r_{\text{BLR}}/ld)^{-\alpha}$ is the correction factor due to the central disc radiation and $\alpha > 0$. So, $v_{\text{cr}}^2 < v_c^2$ for the same radius r_{BLR} , and $v_{\text{FWHM}}^2 \propto v_{\text{cr}}^2 \propto r_{\text{BLR}}^{-1}(r_g)(r_{\text{BLR}}/ld)^{-\alpha}$. Thus, $f \propto r_{\text{BLR}}^{-1}(r_g)/v_{\text{FWHM}}^2 \propto (r_{\text{BLR}}/ld)^{\alpha}$, i.e. $\log f = D + \alpha \log(r_{\text{BLR}}/ld)$, where D is independent of r_{BLR} and M_{\bullet} . The virial factor f is a function of r_{BLR} rather than $r_{\text{BLR}}(r_g)$. α is likely different from one to another AGN and might depend on accretion rates. We have $\alpha \approx 0.3$ for Mrk 110 (see Figure 1). The lines in parallel with the best fit straight line to Mrk 110 cannot connect two points of Mrk 493 or *IRAS* 04416 even considering the corresponding errors. It is obvious that a larger α is needed to connect the two points of Mrk 493 or *IRAS* 04416. Mrk 110, Mrk 493 and *IRAS* 04416 have $\dot{M} = 5.89, 75.9$ and 426.6 or $\dot{M}_f = 0.49, 1.04$ and 7.27 , respectively. Then, Mrk 493 and *IRAS* 04416 have larger α and accretion rates than Mrk 110 has, i.e. α likely depends on accretion rate. The virial factor f is an increasing function of r_{BLR} , and this increasing trend results from the radiation pressure influence on the BLR clouds due to the central accretion disc radiation. For individual AGNs, the radiation pressure due to accretion disc will produce more obvious effect on the BLR clouds as α increases. As α vanishes, the radiation pressure effect also vanishes. These larger f values ≈ 8 –16 will make M_{RM} increase for Mrk 110, with respect to the mass derived from $\langle f \rangle \approx 1$. In like manner, the largening of f may exist in quasars. Quasar J0100+2802 at $z = 6.30$, the most luminous quasar known at $z > 6$, has a black hole mass of ~ 12 billion M_{\odot} and a bolometric luminosity of 1.62×10^{48} ergs s^{-1} (Wu et al. 2015). The largening of f will give a larger mass in J0100+2802. The larger black hole mass further gives rise to the most significant challenge to the Eddington limit growth of black holes in the early Universe (Volonteri 2012; Willott et al. 2010). The larger f values than $\langle f \rangle \approx 1$ will decrease the Eddington ratios. The lower Eddington ratios will set constraints on accretion states.

The blueshifts of [O III] $\lambda 5007$ were found (e.g. Boroson 2005; Bae & Woo 2014; Zhou et al. 2006).

The blueshifts will make it uncertain for the relevant broad line shifts relative to [O III] $\lambda 5007$. Since the reference of broad line shifts is in problem, it will be a good way to avoid using [O III] as the reference. Equation (7) only needs the redshift difference between two broad lines. Thus, the blueshifts of [O III] will not influence the black hole masses derived from equation (7). The consistent two black hole masses derived from equations (4) and (7) for Mrk 110 suggests that the blueshifts of [O III] did not result in obvious influence on the black hole masses derived from equation (4) and the rms spectra. Thus, the broad-line-to-broad-line comparison path (equation[7]) could overcome the limitations of narrow line shifts. Comparisons between M_{grav} of Mrk 110 derived from the broad-line-to-broad-line comparison path and the single broad-line path show that the rms spectra could overcome the limitations of narrow line shifts. The mean spectra might also overcome the limitations of narrow line shifts. Jonić et al. (2016) suggested that the broad line with the red asymmetry can be used to measure z_g , by the shift of the centroid of broad line with respect to its peak. This approach could stride over the limitations of narrow line shifts as the narrow lines are regarded as the reference to measure z_g . Also, the redward shifts of broad lines may be from the BLR cloud inflow, and this explanation seems to be easily understood except that some extra parameters are needed to describe the inflow. Jonić et al. (2016) found significant positive correlations between intrinsic shift Δz_{50} and v_{FWHM} of broad H β and Mg II, $\Delta z_{50} \propto v_{\text{FWHM}}^n$ with $n \approx 2$, for AGNs. These correlations confirm the gravitational redshift origin of the relevant redward shifts. The gravitational redshift is a natural outcome of virialized motions of BLR gas in AGNs. The blueshift is usually obtained for high-ionization broad lines, e.g. C IV, and is considered as a signal of gas outflow that is a natural interpretation of blueshift of high-ionization lines (e.g. Wang et al. 2011, references therein). The outflow may be driven by the radiation pressure of the central accretion disc. Mrk 486 has the redshifted broad Fe II and the blueshifted broad H β (shifted on $\pm 1\sigma$). These two shifted broad lines may be explained in terms of the combination of the outflow and the gravitational redshift effect. The redshifted broad H β and Fe II in other 3 NLS1s might be dominated by the gravitational redshift effect.

IRAS 04416 and Mrk 493 have a mean $r_{\text{BLR}} \sim 900r_g$ and $\sim 2000r_g$, respectively. According to Müller & Wold (2006), the gravitational redshift can be probed out to $r_{\text{BLR}} \sim 900r_g$ and $\sim 2000r_g$ with a resolution of $\approx 8.3 \text{ \AA}$ and $\approx 3.8 \text{ \AA}$, respectively. The spectra measured in the reverberation mapping campaign for SEAMBHs have a resolution of 1.8 \AA (Du et al. 2014; Hu et al. 2015). Thus, the gravitational redshift can be probed out to $r_{\text{BLR}} \sim 900r_g$ and $\sim 2000r_g$, respectively, for *IRAS* 04416 and Mrk 493 with the spectra used to measure the redward shifts of H β and Fe II. The spectral resolution of $\sim 500 \text{ km s}^{-1}$ mentioned in Du et al. (2014) and Hu et al. (2015) is an instrumental broadening that mainly influences width of spectrum line, such as *FWHM*, but slightly influences the central wavelength of spectrum line. The instrumental broad-

ening has been corrected to obtain *FWHM*s of broad lines in NLS1s (Du et al. 2014; Hu et al. 2015). On the basis of the ultraviolet reverberation mapping of carbon lines, a small inclination angle is suggested, supporting a high- f value, for PG 1247+267, the brightest quasar ever analyzed for reverberation with $\lambda L_{\lambda}(1350\text{\AA}) = 3.9 \times 10^{47} \text{ ergs s}^{-1}$ and ionization stratification similar to low-luminosity AGNs (Trevese et al. 2014). There is a redward shift of 0.008 for broad H β with respect to [O III] $\lambda 5007$ in the infrared spectrum (McIntosh et al. 1999b). The broad H β has $v_{\text{FWHM}} = 7460 \text{ km s}^{-1}$ (McIntosh et al. 1999a). Assuming the shift of 0.008 is the gravitational redshift, we have $f \approx 13$. An inclination angle ≈ 8 degrees is derived for PG 1247+267 if the H β BLR has a disc-like geometry. Our results are consistent with those in Trevese et al. (2014). This indicates that the gravitational redshift of H β is reliable on the order of magnitude for PG 1247+267, and the new method is feasible to estimate f in quasars. Mrk 110, other three NLS1s and PG 1247+267 have high- f values and small inclinations of BLRs. It seems that the gravitationally redshifted optical spectrum lines are more easily detected in the AGNs with the nearly face-on viewed BLRs, due to the fact that the competing Doppler effect is weaker than the gravitational redshift effect in the case of the nearly face-on disc-like BLRs (e.g. Müller & Wold 2006).

In this paper, based on the gravitationally redshifted optical broad emission lines in AGNs, a new method is proposed to measure the virial factors f in M_{RM} by using z_g and v_{FWHM} of broad lines. It is difficult to determine f in the reverberation mapping due to the unclear kinematics and geometry of BLRs in AGNs. The different f implies the difference of geometry and kinematics of the BLRs. First, this new method is applied to NLS1 Mrk 110 with the gravitationally redshifted broad lines He II, He I, H β and H α . These four lines have $f \approx 8\text{--}16$ that are distinctly larger than the mean $\langle f \rangle \approx 1$ derived from the $M_{\bullet} - \sigma_{\ast}$ relation. The He II and He I lines have slightly smaller f than do the H β and H α lines. There is a positive correlation between the factor f and the radius r_{BLR} for Mrk 110 (see Figure 1), and this increasing trend can be naturally explained by the radiation pressure influence of accretion disc on the BLR clouds in Mrk 110. The radiation pressure influence seems to be more important than thought usually in AGNs. Second, Seyfert 1 NGC 4593 has $f = 2.9$ derived from the redshifted H α line. Third, NLS1s Mrk 493, *IRAS* 04416 and Mrk 42 have high- f values of several tens derived from the redward shifted optical H β and Fe II lines. In plot of $\log f$ versus $\log r_{\text{BLR}}$, NGC 4593 is below the line best fit to Mrk 110, and both of Mrk 493 and *IRAS* 04416 are above the same line. This difference may result from accretion rate difference. NGC 4593, Mrk 110, Mrk 493 and *IRAS* 04416 have $\mathcal{M} = 0.08, 5.89, 75.9$ and 426.6 or $\mathcal{M}_{\text{f}} = 0.03, 0.49, 1.04$ and 7.27 , respectively. Also, the factor f increases for these four objects. The higher accretion rate may correspond to the larger f in different AGNs. The larger f of four NLS1s suggest the nearly face-on viewed BLRs if their BLRs have a disc-like geometry. The measurements of f from the gravitationally redshifted optical broad lines have the potential to improve M_{RM} . This paper is based on the condition that the optical BLRs are at the distances of hundreds to thousands of r_g away from the central black holes. NGC 4593, Mrk 110, Mrk 493 and *IRAS* 04416 have $r_{\text{BLR}} \sim 2700 r_g, 560\text{--}4000$

r_g , 1700–2400 r_g and 600–1300 r_g , respectively. So, this condition is met and the Schwarzschild metric is applicable to deducing the formulas in section 2. These larger f values derived from the gravitational redshift method can generate the higher black hole masses and the lower Eddington ratios with respect to those in the case of $\langle f \rangle \approx 1$ for AGNs.

ACKNOWLEDGMENTS

We are grateful to the anonymous referee for important comments leading to significant improvement of this paper. We thank the helpful discussions of Dr. H. Q. Li, Dr. P. Du and Dr. F. Wang. HTL thanks the National Natural Science Foundation of China (NSFC; grants 11273052 and U1431228) for financial support. JMB acknowledges the support of the NSFC (grant 11133006). HTL also thanks the financial supports of the project of the Training Programme for the Talents of West Light Foundation, CAS and the Youth Innovation Promotion Association, CAS.

REFERENCES

- Bae H. J., Woo J. H., 2014, *ApJ*, 795, 30
 Barth A. J. et al., 2011, *ApJ*, 743, L4
 Barth A. J. et al., 2015, *ApJS*, 217, 26
 Bentz M. C. et al., 2006, *ApJ*, 651, 775
 Blandford R. D., McKee C. F., 1982, *ApJ*, 255, 419
 Boroson T., 2005, *AJ*, 130, 381
 Carswell R. F. et al., 1991, *ApJ*, 381, L5
 Denney K. D. et al., 2010, *ApJ*, 721, 715
 Dietrich M. et al., 1994, *A&A*, 284, 33
 Du P. et al. (SEAMBH Collaboration), 2014, *ApJ*, 782, 45
 Du P. et al. (SEAMBH Collaboration), 2015, *ApJ*, 806, 22
 Du P. et al. (SEAMBH Collaboration), 2016, *ApJ*, 820, 27
 Fabian A. C., Rees M. J., Stella L., White N. E., 1989, *MNRAS*, 238, 729
 Fabian A. C., Iwasawa K., Reynolds C. S., Young A. J., 2000, *PASP*, 112, 1145
 Haas M., Chini R., Ramolla M., Pozo Nuñez, F., Westhues C., Watermann R., Hoffmeister V., Murphy M., 2011, *A&A*, 535, A73
 Hu C. et al. (SEAMBH Collaboration), 2015, *ApJ*, 804, 138
 Jonić, S., Kovačević-Dojčinović, J., Ilić, D., Popović, L. Č., 2016, *Ap&SS*, 361, 101
 Kaspi S., Netzer H., 1999, *ApJ*, 524, 71
 Kaspi S., Smith P. S., Netzer H., Maoz D., Jannuzi B. T., Givon U., 2000, *ApJ*, 533, 631
 Kaspi S., Brandt W. N., Maoz D., Netzer H., Schneider D. P., Shemmer O., 2007, *ApJ*, 659, 997
 King A. L. et al., 2015, *MNRAS*, 453, 1701
 Kollatschny W., Dietrich M., 1997, *A&A*, 323, 5
 Kollatschny W., Bischoff K., Robinson E. L., Welsh W. F., Hill G. J., 2001, *A&A*, 379, 125
 Kollatschny W., 2003a, *A&A*, 407, 461
 Kollatschny W., 2003b, *A&A*, 412, L61
 Krolik J. H., Horne K., Kallman T. R., Malkan M. A., Edelson R. A., Kriss G. A., 1991, *ApJ*, 371, 541
 Krolik J. H., 2001, *ApJ*, 551, 72
 McIntosh D. H., Rieke M. J., Rix H. W., Foltz C. B., Weymann R. J., 1999a, *ApJ*, 514, 40
 McIntosh D. H., Rix H. W., Rieke M. J., Foltz C. B., 1999b, *ApJ*, 517, L73
 McLure R. J., Dunlop J. S., 2001, *MNRAS*, 327, 199
 Müller A., Wold M., 2006, *A&A*, 457, 485
 Nishihara E., Yamashita T., Yoshida M., Watanabe E., Okumura S., Mori A., Iye M., 1997, *ApJ*, 488, L27
 Onken C. A., Ferrarese L., Merritt D., Peterson B. M., Pogge R. W., Vestergaard Ma., Wandel A., 2004, *ApJ*, 615, 645
 Pei L. et al., 2014, *ApJ*, 795, 38
 Peterson B. M., 1993, *PASP*, 105, 247
 Peterson B. M. et al., 2004, *ApJ*, 613, 682
 Peterson B. M. et al., 2005, *ApJ*, 632, 799
 Piotrovich M. Y., Gnedin Yu. N., Silant'ev N. A., Natsvlshvili T. M., Buliga S. D., 2015, *MNRAS*, 454, 1157
 Popovic L. C., Vince I., Atanackovic-Vukmanovic O., Kubicela A., 1995, *A&A*, 293, 309
 Pozo Nuñez, F., Ramolla M., Westhues C., Bruckmann C., Haas M., Chini R., Steenbrugge K., Murphy M., 2012, *A&A*, 545, A84
 Press W. H., Teukolsky S. A., Vetterling W. T., Flannery B. P. 1992, *Numerical Recipes* (2nd ed.; Cambridge: Cambridge Univ. Press)
 Rees M. J., 1984, *ARA&A*, 22, 471
 Rees M. J., Begelman M. C., Blandford R. D., Phinney E. S., 1982, *Nature*, 295, 17
 Reynolds C. S., Nowak M. A., 2003, *Phys. Rep.*, 377, 389
 Riess A. G. et al., 2004, *ApJ*, 607, 665
 Shen Y. et al., 2015a, *ApJS*, 216, 4
 Shen Y. et al., 2015b, *ApJ*, 805, 96
 Shen Y. et al., 2016, *ApJ*, 818, 30
 Spergel D. N. et al., 2003, *ApJS*, 148, 175
 Tanaka Y. et al., 1995, *Nature*, 375, 659
 Tremaine S., Shen Y., Liu X., Loeb A., 2014, *ApJ*, 794, 49
 Trevese D., Perna M., Vagnetti F., Saturni F. G., Dadina M., 2014, *ApJ*, 795, 164
 Vanden Berk, D. E. et al., 2001, *AJ*, 122, 549
 Volonteri M., 2012, *Science*, 337, 544
 Wandel A., Peterson B. M., Makkan M. A., 1999, *ApJ*, 526, 579
 Wang H. Y. et al., 2011, *ApJ*, 738, 85
 Wang J. M. et al. (SEAMBH Collaboration), 2014, *ApJ*, 793, 108
 Willott C. J. et al., 2010, *AJ*, 140, 546
 Woo J. H., Urry C. M., 2002, *ApJ*, 579, 530
 Woo J. H., Yoon Y., Park S., Park D., Kim S. C., 2015, *ApJ*, 801, 38
 Wu X. B. et al., 2015, *Nature*, 518, 512
 Zheng W., Sulentic J. W., 1990, *ApJ*, 350, 512
 Zhou H. Y. et al., 2006, *ApJS*, 166, 128